CO_2 Solubility in Aqueous Electrolyte Solutions Confined in Calcite Nanopores

Azeezat Ali and Alberto Striolo*

Department of Chemical Engineering, University College London, London WC1E 6BT United Kingdom

David R. Cole

School of Earth Sciences, The Ohio State University, Columbus, Ohio 43210

United States of America

ABSTRACT

Geological carbon dioxide sequestration in deep saline aquifers can play a key role in the successful mitigation of greenhouse gas emissions. Several conditions have been identified that affect the solubility of CO_2 in water, including temperature, pressure, pH and salinity. At similar conditions, the solubility in bulk fluids differs from the solubility in confined porous media. We conducted equilibrium molecular dynamics simulations to investigate the solubility of CO_2 in water confined in slit-shaped calcite pores. We studied the effects of brine (NaCl and $MgCl_2$) and compared our results to the corresponding bulk solubility. Compared to bulk water/brine, the solubility of CO_2 is lower in calcite pores and decreases as the pores narrow. Adsorption energy calculations were performed to compare our results to CO_2 solubility in water-filled silica pores. These results indicate that narrower calcite pores are less attractive for the adsorption of CO_2. In addition, the simulation results suggest that the difference in the positions where the ions adsorb also affects whether salts increase or decrease the solubility of CO_2 in confined water. Confinement and ions also reduce the mobility of CO_2 in water. These observations contribute to the design of long-term CO_2 sequestration strategies as they provide boundary constraints for the amount of CO_2 that can dissolve in hydrated pores, as well as the timing of CO_2 transport in such systems.

* Corresponding Author: a.striolo@ucl.ac.uk

1. INTRODUCTION

Dissolution of CO_2 in saline aquifers is recognized as one of the viable options for subsurface storage of large quantities of CO_2. The efficiency of dissolution depends on several conditions such as temperature, pressure, and ionic composition.[1,2] Salts can induce either salting-out or salting-in effects in relation to the reduction or increase, respectively, in the gas solubility. These effects, dependent on the ionic size and charge, are generally attributed to the difference in the interactions between ions and water in comparison to the gases and water. Several experimental studies reported that salts generally reduce solubility of CO_2 in bulk water, with divalent ions having stronger effects than monovalent ions.[3-8]

Ho and Ilgen[9] used MD simulations to provide a different perspective on the origin of the electrolytes effects on the solubility of CO_2 in a bulk solution. They presented the free energy of dissolution (hydration energy) as the sum of the work required to form a cavity to accommodate the gas molecule and the interaction energy between CO_2 and the solvent. Although increasing salinity leads to more negative interaction energies between CO_2 and the aqueous solutions, they found that the formation of cavities is the main mechanism controlling CO_2 dissolution. In particular, increasing the concentration of salts reduces the probability of cavity formation (which leads to salting out). They also reported that the magnitude of the interaction energies in solutions containing monovalent ions were lower than in those containing divalent ions, alluding to stronger interactions between CO_2 and divalent ions.

It is also known that confinement affects solubility. Phan et al.[10,11] employed MD simulations to study the methane solubility in water confined in silica, alumina and magnesium oxide (MgO) nanopores. They found higher solubility in confinement, which was related to the higher probability of 'cavity formation' within confined water. Ho et al.[12] reported over-solubility of CO_2, N_2, and CH_4 in water confined in ZSM-5, MCM-41, and MIL-100 nanopores, compared to the bulk fluid. They attributed the extent of increase in solubility to the strong affinity of the gases for the solid, as well as to the polarizability of the gases. Other possible mechanisms leading to over-solubility in systems with weak gas-adsorbent interactions are the presence of gases (solute) in regions of low solvent densities and the adsorption of gases at the gas-liquid solvent interface of partially filled pores, which was found to affect the free energy of solvation. Diaz Campos et al.[13] observed an enhancement in the solubility of methane in water confined in graphene pores and they reported that the solubility is very sensitive to the wettability of the pore walls. Luzar and Bratko[14,15] also reported an increase in the solubility of CO_2, O_2, Ar and

N_2 in hydrophobic confinement. Pera-Titus et al.[16] experimentally observed the increase in the solubility of H_2 in $CHCl_3$, CCl_4, n-hexane, ethanol, and water when confined in γ-alumina, silica, and MCM-41. In contrast, Badmos et al.[17] found that confinement reduces the solubility of hydrogen sulphide (H_2S) in water confined in silica nanopores. It should be pointed out that in many molecular simulation studies, CO_2, H_2S and other species are not allowed to protonate upon dissolution in water, and that the mineral surfaces are not allowed to respond to system pH via protonation/de-protonation of their surface sites, which constitute approximations necessary because of the high computing cost required to account for such physical phenomena within the molecular models. The validity of these approximations can be assessed by comparing simulation results to experiments. For example, Liu et al.[18] reported, through Monte Carlo simulations, that the prediction of CO_2 solubility in water is within reasonable margins from experimental data. The deviations were linked to accuracy of the cross-term interaction parameters. Moreover, the concentration of H_2CO_3 and other species are at least two orders of magnitude smaller than the dissolved CO_2 concentration.[19,20] Gadikota et al.[21] documented, via simulations and experiments, the increase in the solubility of CO_2 and noble gases (Ne, Ar and Kr) in water confined within Na-montmorillonite clay nanopores. Similar observations were reported by Botan et al.[22] in their study of CO_2 in water in Na-montmorillonite clay interlayers. Li et al.[23] studied the solubility of CO_2 in water confined in kaolinite nanopores and found CO_2 under-solubility in hydrophilic pores and over-solubility in hydrophobic pores. On the hydrophilic face of kaolinite, water adsorbs strongly on the pore surfaces, preventing the adsorption of CO_2. In hydrophobic pores, both CO_2 and water can adsorb. This observation is consistent with observations reported by Tenney and Cygan,[24] according to which CO_2 can form a non-wetting droplet on the hydrophilic surface of kaolinite while both CO_2 and H_2O interact directly with the hydrophobic surface of the mineral. Li et al.[25] found that CO_2 is generally more soluble in water confined in silica pores than in bulk and that solubility decreases as the concentration of NaCl and system pH increase.

Despite the importance of depleted hydrocarbon reservoirs hosted by carbonate-bearing formations, a possible target for geological carbon sequestration, there have been only a limited number of studies on the solubility of gases in water confined within these porous materials. To fill this knowledge gap, this paper explores the influence of monovalent and divalent salts (NaCl and $MgCl_2$) and pore width on the solubility of CO_2 in water confined in calcite. Na and Mg salts are chosen because our prior simulation results suggest that they accumulate preferentially at different locations with respect to the hydrated calcite surface. The

interpretation of a variety of experimental and molecular dynamics simulation data in the literature also suggests that NaCl is a 'structure breaker', while $MgCl_2$ is considered a 'structure maker' suggesting perhaps different effects on CO_2 solubility in confined water.[26-30] We compare the results to bulk CO_2 solubility in aqueous electrolyte solutions, as well as to literature results for CO_2 solubility in water confined in other materials.

The rest of the manuscript is structured as follows: In the Simulation Methodology, we describe force fields, simulation set up and algorithms used. In the Results section we provide detailed analyses of our results through atomic density profiles, solubility calculations, diffusion coefficients and adsorption energies. We then conclude with a summary of our main findings.

2. SIMULATION MODELS AND METHODOLOGY

2.1. Confined Systems

The calcite slab, with thickness 1.366 nm, was obtained from a calcite crystal terminated at the $10\bar{1}4$ plane.[31] In our model, calcium and carbon atoms were kept rigid, while the oxygen atoms were allowed to vibrate. The slab was placed within the simulation box in an orientation parallel to the X-Y plane, with X and Y dimensions of the surface 9.714 x 9 nm^2. The calcite pore was obtained by placing two calcite slabs at distances corresponding to the pore width. The Z dimensions of the simulation box were 4.732, 5.232, 5.532 and 5.732 nm for pores of width 2.0, 2.5, 2.8 and 3.0 nm, respectively. Note that the pore is in contact with the bulk reservoir along the Y direction, while it is infinite (because of periodic boundary conditions) along the X direction. The initial configuration of the confined system was created by placing enough water molecules and salt ions in the bulk region on both sides of the pore to fill it, with thin water films at the entrances of the pore (see Figure 1). CO_2 molecules were then placed in the bulk region, to adsorb into the pore as the simulation progresses. At equilibrium, the CO_2 molecules in the pore indicate the solubility in water. The compositions of all the systems studied are provided in Table 1. The simulations were performed under periodic boundary conditions in all three directions. However, the calcite slab was finite along the Y direction since the simulation box was elongated to 21 nm, to allow for unconfined (bulk) regions on either side of the slab, as illustrated in Figure 1.

The Peng-Robinson equation of state (EOS) was applied to estimate the bulk pressure of the system from the density of CO_2 outside the pore once equilibrium conditions were achieved. Note that the EOS was applied on the 'pseudo' bulk values for our systems, hence it is believed to yield reasonable results. The calculated pressures of each system are presented in Table 2. These values should be considered as estimates for the bulk phase pressure in equilibrium with the pore pressure. Because the generally accepted target depth for geological CO_2 sequestration is set at ~ 800 m, the temperature and pressure conditions considered in this work are chosen to represent depths of about 1000 meters in saline aquifers.[32] To relate the pressure shown in Table 2 to CO_2 sequestration protocols, it might be beneficial to recall that the experimental bulk critical pressure and critical temperature for CO_2 are 7.38 MPa and 304.21 K, respectively.[33] The model implemented here to simulate CO_2 yields critical pressure and critical temperature of 7.39 MPa and 304.04 K, respectively[34]

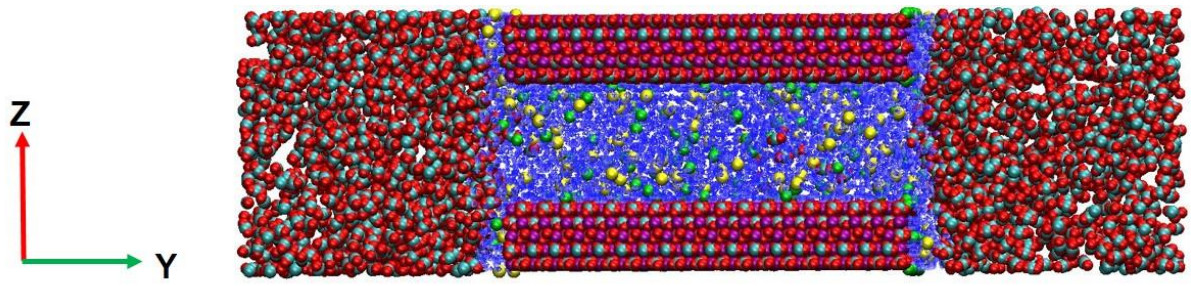

Figure 1. Representative simulation snapshots of the calcite nanopore filled with water and NaCl or $MgCl_2$ ions, with CO_2 outside the pores in the bulk region. Ca = purple; C = cyan; O = red; H = white; Na, Mg = yellow; Cl = green. Water molecules are shown in blue.

Table 1. Composition of the systems used in equilibration simulations within the configuration shown in Figure 1. These simulations were conducted at 303 and 323 K.

Salinity	**Pore width (nm)**	**Number of molecules**		
		H_2O	CO_2	Salt ions
0	2	3400	1600	-
0	2.5	4400	1800	-
0	2.8	4760	1800	-
0	3	5000	2000	-
1.5 M NaCl	3	5000	2000	136
1.5 M $MgCl_2$	3	5000	2000	136

Table 2. Bulk Pressures for all systems simulated at 303 K and 323 K.

Salinity	Pore width (nm)	Pressure (MPa)	
		303 K	323 K
0	2.5	7.25 ± 0.01	10.43 ± 0.01
0	2.8	7.22 ± 0.01	10.09 ± 0.02
0	3	7.25 ± 0.01	10.5 ± 0.3
1.5 M NaCl	3	7.25 ± 0.01	10.8 ± 0.1
1.5 M $MgCl_2$	3	7.24 ± 0.01	10.7 ± 0.15
0	Bulk	6.84 ± 0.02	8.15 ± 0.15
1.5 M NaCl	Bulk	6.92 ± 0.01	8.44 ± 0.04
1.5 M $MgCl_2$	Bulk	6.94 ± 0.04	8.6 ± 0.25

To analyse structural and transport properties of fluids confined within the various pores, the pore was rendered infinite by removing the unconstrained (bulk) regions from the final configuration of the system at equilibrium and implementing periodic boundary conditions in all directions. For these systems, the resultant dimensions of the simulation system were equal to those of the calcite pore. The compositions of the systems, presented in Table 3, reflect the composition of the pore fluid at equilibrium.

Table 3. Composition of confined calcite systems simulated at 303 K and 323 K.

Salinity	Pore width (nm)	Number of molecules					
		303 K			323 K		
		H_2O	CO_2	Salt ions	H_2O	CO_2	Salt ions
0	2.5	3466	4	-	3453	3	-
0	2.8	3790	13	-	3784	11	-
0	3	4013	23	-	4013	23	-
1.5 M NaCl	3	3929	21	106	3892	16	105
1.5 M $MgCl_2$	3	3792	22	103	3761	21	102

2.2. Pseudo Bulk Systems

To compare the solubility of CO_2 in confined fluids to that predicted in the bulk, we placed 530 water molecules in a 2 x 4 x 2 nm^3 simulation box. 14 salt ions were added to achieve the concentration of 1.5 M. Replicating the confined systems simulations, 200 CO_2 molecules were placed on either side of the aqueous film, to increase the length of the slab in the y-direction to 12 nm (see Figure 2). The bulk pressure was estimated with the Peng-Robinson EOS, applied to the properties (density, temperature and composition) of the pseudo bulk phases. To analyse

structural and dynamical properties of CO_2 and water in the bulk, we conducted additional simulations in the absence of water-CO_2 interfaces. The composition of these bulk liquid simulations, shown in Table 4, was determined from the equilibrated systems used to estimate CO_2 solubility in bulk.

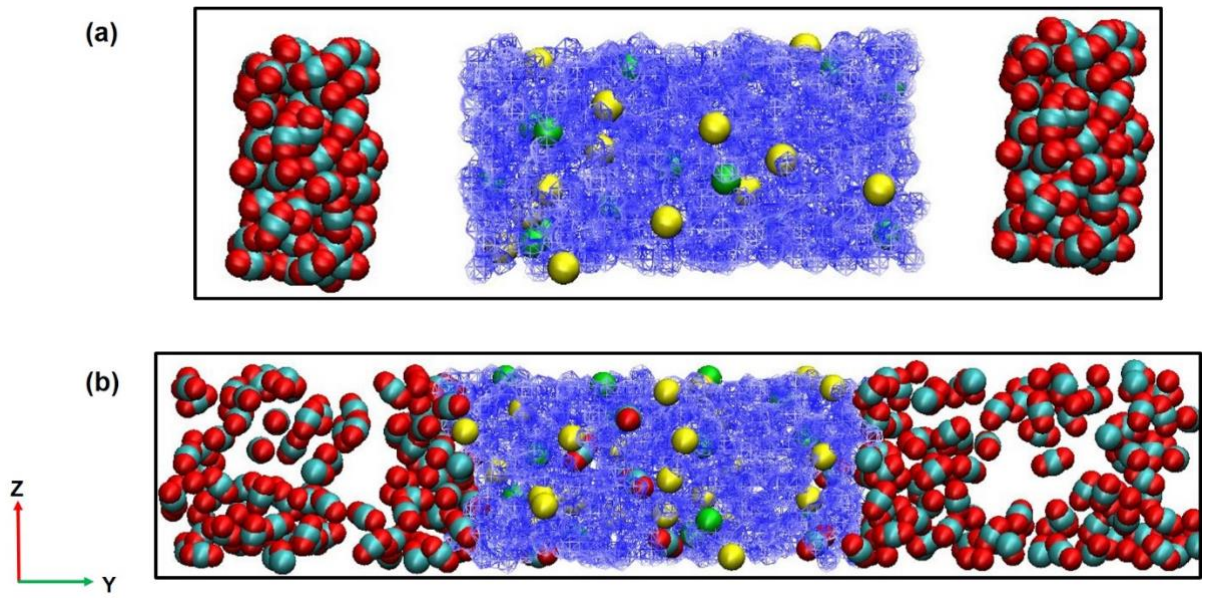

Figure 2. (a) Initial and (b) final configurations for the pseudo-bulk systems. C = cyan; O = red; H = white; Na, Mg = yellow; Cl =green. Water molecules are shown in blue.

Table 4. Composition of simulated bulk systems.

Salinity	**Number of molecules**					
	303 K			323 K		
	H_2O	CO_2	Salt ions	H_2O	CO_2	Salt ions
0	2112	38	-	2112	35	-
1.5 M NaCl	2041	19	55	2029	16	55
1.5 M $MgCl_2$	1939	17	53	1920	16	52

2.3. Force fields

We described calcite in our simulations using the force field developed by Xiao et al.[35] In our recent work,[36] we discussed the structure of interfacial water on calcite when this force field is used. The rigid simple point charge extended (SPC/E)[37] and Joung-Cheatham (JC)[38] force fields were used to describe water and NaCl, respectively. Electronic Continuum Correction (ECC) forcefields developed for magnesium[39] and chloride[40] ions were used to describe $MgCl_2$. This forcefield improves significantly the description of the structure of the multivalent ions in

electrolyte solutions compared to standard approaches.[39-41] It should be noted that these force fields were developed consistently with the SPC/E model of water.

For CO_2, we used the EPM2 model with bond stretching and angle bending from Cygan et al.[42] In comparison to rigid models, including flexibility improves the predictions of the interfacial and thermodynamic properties and correctly predict the vibrational spectra of CO_2.[42-44] Cygan et al.[42] found that the CO_2-water radial distribution functions from simulations are consistent with literature. In addition, incorporating flexibility allows for better prediction of CO_2 diffusion coefficients in water, when compared with experiments.[45]

In our simulations, following conventional protocols, dispersive and electrostatic forces were modelled by the 12–6 Lennard-Jones (LJ) potential and the Coulombic potential, respectively. The LJ parameters for unlike atomic interactions were obtained using the Lorentz-Berthelot mixing rule.[46] The cut-off distance for all interatomic interactions was set to 12 Å; long-range electrostatic interactions were calculated using the particle mesh Ewald (PME) method.[47]

2.4. Approximations. It should be noted that the atomistic models implemented in this work are not allowed to dissociate nor protonate. Therefore, CO_2 does not yield carbonic acid nor bicarbonate when dissolved in water, and the system pH does not change during the simulations. The fact that aqueous solutions containing $MgCl_2$ are slightly more acidic than those containing NaCl, whose pH is 7, is also not taken into consideration. The mineral surface is not allowed to react with water, and the system composition is maintained below the saturation limit of the NaCl and $MgCl_2$ salts, as necessary since we are not considering the possibility of the formation of carbonate salts.[39,48]

2.5. Algorithms. The simulations were conducted with the GROMACS (version 5.1.4)[49,50] package in the canonical NVT ensemble. The temperature of each system was maintained at 303 K or 323 K using the Nosé-Hoover thermostat[51,52] with a relaxation time of 100 fs. The SETTLE algorithm[53] was used to keep bonds and angles within the water molecules fixed. The confined systems were equilibrated for 200 ns to increase the reliability of the results. Subsequently, production runs of 10 ns were conducted to obtain the density profiles of molecules in the system. The CO_2 densities in the pore oscillated around constant values and both energy and temperature of the system remained within 10% of their average values, confirming equilibrium was achieved. For further analysis, the pore was rendered infinite and equilibrated for 50 ns with the last 4 ns used for data analysis. The pseudo-bulk and bulk systems were equilibrated for 60 ns, followed by a production run of 4 ns.

3. RESULTS AND DISCUSSION

3.1. Atomic Density Profiles

The atomic density profiles for oxygen atoms of water molecules (OW), carbon atoms of CO_2 (C), and the center of the spherical ions (Na^+, Mg^{2+}, Cl^-) were computed along the z direction, perpendicular to the calcite surface. The center of the pore corresponds to the point z = 0.

In Figure 3a, we present the OW and C atomic density distributions within the 3 nm calcite pore. The density profile for water does not change significantly at the two temperatures considered, thus, we only show one profile for clarity. The results reveal the formation of four hydration layers on each surface, with two distinct peaks at distances corresponding to 2.35 Å and 3.25 Å from the calcite substrate. The densities of these peaks show that a large number of water molecules accumulate near the calcite surface. In comparison, the C density profile in the 3 nm calcite pore is characterized by a single, less pronounced peak at ~ 6.15 Å from the surface, which is in between the third and fourth hydration layers. As a result of the strong interactions between the calcite surface and water, CO_2 cannot adsorb any closer to the substrate. Compared to the density profile of CO_2 at 303 K and 7.24 MPa, at 323 K (~10 – 11 MPa), there is a slight reduction in the density of CO_2 adsorbed in the pore, suggesting a reduction in the solubility of CO_2 in water as the temperature increases. Similar calculations were made for fluids in 2.5 nm and 2.8 nm pores, with the results provided in Figures 3b and 3c. The density profile for oxygen atoms of water in both pores are consistent with the results obtained in the 3 nm calcite pore, showing that the hydration structure in the pore is unaffected by a reduction in the pore width from 3 nm to 2.5 nm. For CO_2, while the profile remains qualitatively similar as the pore width changes, there is a reduction in the density as the pore size is reduced.

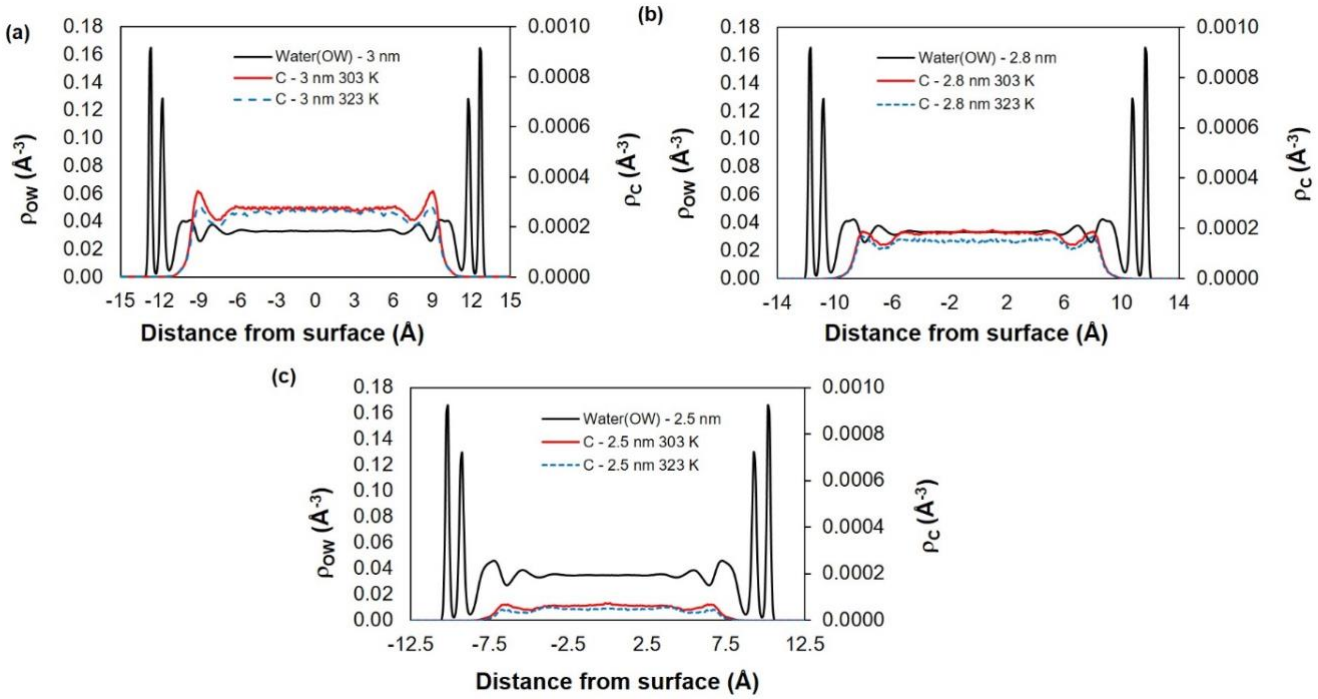

Figure 3. Atomic density profiles along the z direction, vertical from the surface, for oxygen atoms of water (OW, black line) and carbon atoms of CO_2 (C) at temperatures 303 K (red line) and 323 K (blue dotted line), in the (a) 3 (b) 2.8 and (c) 2.5 nm wide calcite pores.

To assess the effects of salt ions on the solubility of CO_2, the density profiles of fluids and ions in the 3 nm calcite pores with NaCl and $MgCl_2$ are reported in Figure 4a and 4b. Because, within the conditions chosen here, temperature has no significant effect on the density profiles of water oxygen and salt ions, only one profile for each component is shown. The addition of salts is found to not affect the water density profile significantly. The density profile of Na^+ ions shows strong ion adsorption at 2.85 Å from the surface, between the first and second hydration layers. Because of their strong hydration shells, the first peak for Mg^{2+} ions is found further away from the surface at 5.05 Å. Cl^- ions in systems with NaCl adsorb at 4.85 Å, to form an electric double layer (EDL) with the Na^+ ions. In systems with $MgCl_2$, the first peak of the Cl^- ion density profile is in the same layer as Mg^{2+} ions.

In the presence of NaCl ions (Figure 4c), there is a reduction in the number of CO_2 adsorbed in the pore, as shown by the reduction in the density of CO_2 in the middle of the pore. While in systems with NaCl, the density of the single density peak representative of CO_2 is unchanged, in the presence of $MgCl_2$, we observe an increase in the density of CO_2 in the pore.

There could be due to electrostatic interactions between Mg^{2+} ions around the CO_2 layer and oxygen atoms of CO_2.

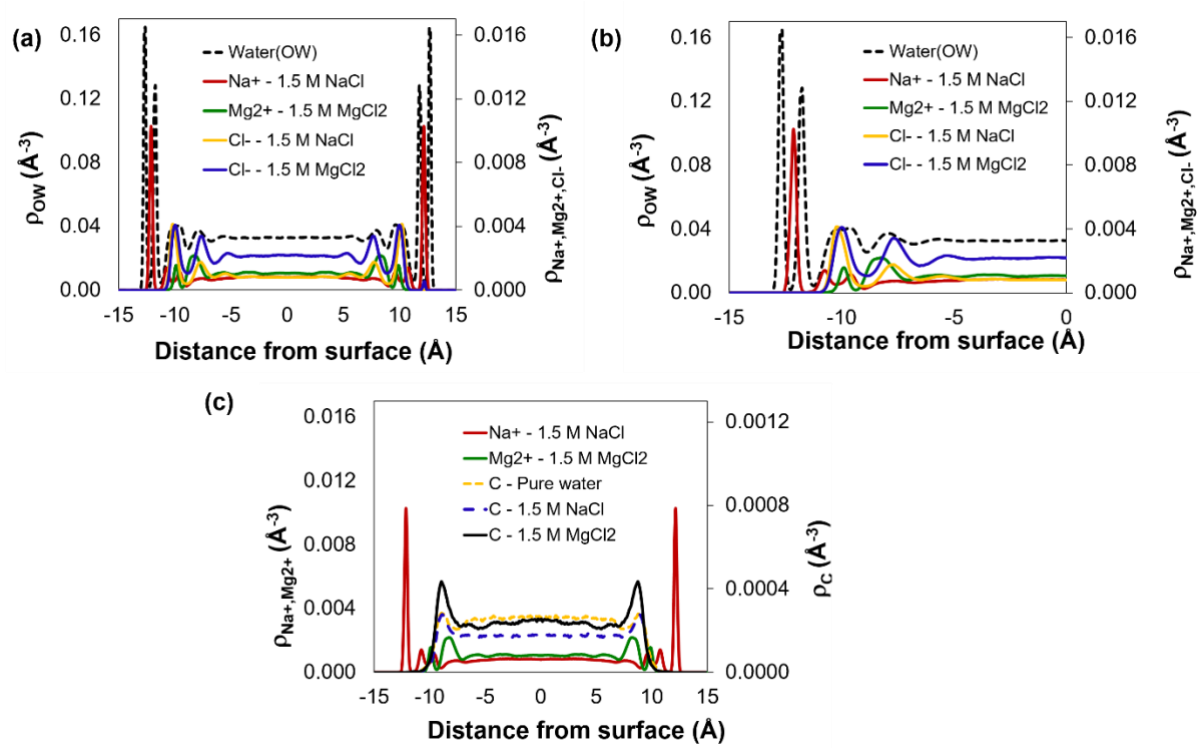

Figure 4. (a) Density profiles of NaCl and $MgCl_2$ ions throughout the pore, (b) Enlarged density profile showing half of the pore to highlight the distributions of atoms/ions on the surface and (c) Carbon atoms of CO_2 along the direction perpendicular to the 3 nm calcite surface. The simulations were conducted at 323 K.

3.2. CO_2 Solubility

We quantified the solubility of CO_2 in confined water as the ratio of the number of CO_2 molecules adsorbed to that of water molecules present in the pore:[10,12,17]

$$Solubility = \frac{Number\ of\ solubilized\ molecules}{Number\ of\ solvent\ molecules} \quad (1)$$

To account for the effects of pore entrances, we excluded 1 nm from either side of the pores in our analysis. The solubility of CO_2 in bulk water was also calculated following the same procedure. The results, presented in Tables 5 and 6, show that the solubility of CO_2 in confined water is lower than the corresponding solubility in bulk water, and decreases as the width of the pore gets narrower. The uncertainty was estimated by applying the standard error calculation method. In the 3 nm pore, the solubility of CO_2 is almost three times lower than

that in the bulk, suggesting that solubility decreases as pore width decreases. Although we performed simulations with 2 nm calcite pores, we observed that after 200 ns, there was no CO_2 present in the pore, suggesting that CO_2 solubility is negligible at these conditions. This was unexpected, given that CO_2 is soluble in bulk water and that several reports in the literature highlight conditions at which various gases are more soluble in confined water than they are in bulk water.[10-16,23,25] We attribute this result to the high water density in the first two hydration layers on calcite, and to the fact that dissolved CO_2 seems to accumulate further from the calcite surface. In our prior work, we reported that CH_4 solubility increases in water confined within ~ 1 nm -wide pores carved out of several minerals, those results were attributed to the presence of molecular-sized cavities, as well as to pronounced fluctuations in the molecular density of confined water.[11] In our prior work[17], we also reported reduced solubility of confined H_2S, which was explained by the perturbation of the hydration structure of this gas upon narrow confinement.[17] Within the pore widths explored here, we found that the hydration structure of CO_2 does not change significantly (results not shown for brevity). Because the structure of hydration water on the mineral surface seems to affect CO_2 solubility in confinement so strongly, it is expected that small changes in the atomic features of the pore surfaces could lead to strong variations in the solubility of CO_2 in water confined in nanopores.

We observed that NaCl has the effect of reducing the solubility of CO_2 in confined water. However, Mg^{2+} ions lead to a slight increase in solubility, consistent with the atomic density profiles observed in Figure 4c. Since Mg^{2+} ions adsorb further away from the pores, their interactions with CO_2 could attract more CO_2 into the pore. In bulk water however, both NaCl and $MgCl_2$ lead to a reduction in solubility. This observation demonstrates that the positions of ions in the pore impact the uptake and solubility of CO_2. In Figure 5, we present a plot of the solubility of CO_2 as a function of pore size in systems with pure water; fitting the results, we estimate that at approximately 2.35 nm and 323 K, the CO_2 solubility becomes zero in water confined within slit-shaped calcite pores. At 303 K, the solubility approaches zero at a somewhat smaller pore width.

Table 5. Solubility of CO_2 in Water and Brine Confined in Calcite Pores.

Temperature (K)	Pore Size (nm)	Salinity	Bulk Pressure (MPa)	Solubility x 10^3
303	3	0	7.25 ± 0.00	5.79 ± 0.25
		1.5 M NaCl	7.25 ± 0.00	5.60 ± 0.14
		1.5 M $MgCl_2$	7.24 ± 0.00	5.94 ± 0.33
	2.8	0	7.22 ± 0.00	3.63 ± 0.14
	2.5	0	7.25 ± 0.00	1.22 ± 0.11
323	3	0	10.51 ± 0.26	5.71 ± 0.61
		1.5 M NaCl	10.83 ± 0.06	4.03 ± 0.19
		1.5 M $MgCl_2$	10.74 ± 0.10	5.81 ± 0.33
	2.8	0	10.09 ± 0.02	2.66 ± 0.16
	2.5	0	10.43 ± 0.01	0.31 ± 0.07

Table 6. Solubility of CO_2 in Bulk Water and Brine Systems.

Temperature (K)	Salinity	Bulk Pressure (MPa)	Solubility x 10^3
303	0	6.84 ± 0.02	18.06 ± 0.25
	1.5 M NaCl	6.92 ± 0.01	9.28 ± 1.51
	1.5 M $MgCl_2$	6.94 ± 0.04	8.46 ± 0.99
323	0	8.16 ± 0.11	16.6 ± 0.76
	1.5 M NaCl	8.44 ± 0.04	8.89 ± 0.40
	1.5 M $MgCl_2$	8.57 ± 0.20	8.32 ± 0.10

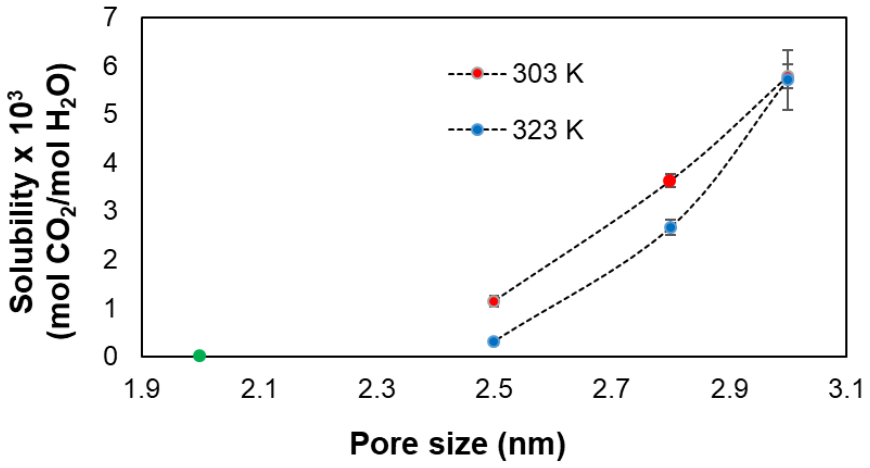

Figure 5. CO_2 solubility in pure water versus calcite pore size for 2.5 – 3 nm pores simulated at 303 (red circles) and 323 K (blue circles). Lines are a guide to the eye. The green circle represents the solubility of CO_2 in the 2nm pores at both temperatures.

To understand the contribution of the calcite surface to the CO_2 solubility, we divided the pore into three regions to calculate the solubility in each location. Figure 3 can be used as a guide. region 1 ($z < 3.75$ Å) corresponds to the first two hydration layers close to the pore, where there are no CO_2 molecules adsorbed. In regions 2 and 3, we find the first CO_2 layer and middle of the pore, respectively. We calculated the volume of each region and observed that for a slit-shaped pore of width 3 nm, ~25% of the pore (region 1) is unavailable to CO_2. As the pore width decreases, the fraction of the pore volume not accessible to CO_2 increases. Our further analysis focuses on regions 2 and 3 in the systems at 323 K. In Table 7, we report the solubility of CO_2 in these regions for the various pores. While the solubility of CO_2 is higher in the middle of the pore compared than that obtained nearer to the pore surfaces, the value does not converge to the solubility of CO_2 in bulk water for the systems simulated here. This indicates that the fluid behaviour throughout the pore differs from bulk properties. In systems with NaCl, there is a reduction in solubility in both regions 2 and 3, compared to systems with pure water. Conversely, in region 2, the presence of Mg^{2+} ions leads to an increase in solubility.

Table 7. CO_2 Solubility in Water and Brine Confined in Calcite Pores at 323 K.

	CO_2 Solubility x 10^3	
Pore size	region 2	region 3
2.5 nm (pure water)	0.22	0.57
2.8 nm (pure water)	2.47	4.03
3 nm (pure water)	4.94	8.51
3 nm (1.5 M NaCl)	4.35	5.57
3 nm (1.5 M $MgCl_2$)	7.04	7.65

3.3. Adsorption Energies

In an attempt to explain the differences in solubility in different mineral pores, which we surveyed in the introduction, we calculated the adsorption energy of one CO_2 molecule in the pores filled with pure water. By applying the two-box method proposed by Heinz,[54] we calculated the difference between the total energy of the system when one molecule of CO_2 is adsorbed in the pore (E_1) and the total energy when CO_2 is outside the pore (E_2). Strong attractive interactions between CO_2 and the pores filled with water are shown by negative adsorption energies. We ran 15 – 20 simulations for each configuration. The adsorption energies (ΔE_{ads}) of CO_2 in calcite pores of width 2.0, 2.5, 2.8, and 3.0 nm are presented in Figure 6. For comparison, we also ran simulations for water confined in silica pores of width 3 nm, following the algorithms described elsewhere,[55] following similar procedure described in the simulation methods section.

$$\Delta E_{ads} = E_1 - E_2 \qquad (2)$$

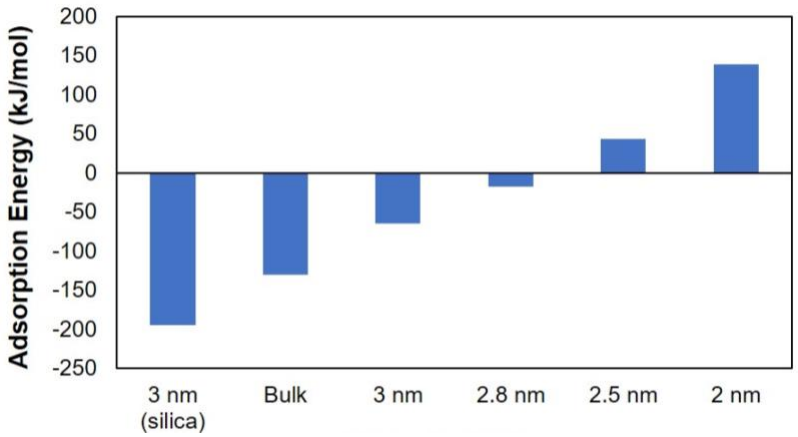

Figure 6. Adsorption energies of one CO_2 molecule in water filled calcite (2 – 3 nm) and silica (3nm) pores, as well as in bulk water. These simulations were conducted at 323 K.

The results in Figure 6 show that CO_2 adsorbs more strongly in the hydrated silica pore than the hydrated calcite pore, which is consistent with our solubility results as well as with the results reported by Li et al.[25] In calcite, as the pore width reduces, the adsorption energy increases, indicating weaker and weaker attraction between CO_2 and the water-filled pore. At 2.5 nm, the adsorption energy is positive, which explains the very low solubility observed at subsequently smaller pore widths. This outcome agrees with the reduction in solubility with decreasing pore size. In Figure 7, we report the correlation between the solubility of CO_2 in pure water and the adsorption energies, which suggests it might be possible to estimate CO_2 solubility in water confined in various minerals by estimating the adsorption energy.

However, our results also show that the interactions between water and the mineral surface play an important role on the adsorption of CO_2 in the pores, as was the case for the diffusion of CH_4 through pores filled with water.[56] We can infer that water has stronger interactions with calcite than silica. Additionally, we determined the interaction energy (E_{int}) between water and the mineral surfaces. This was evaluated as the sum of the electrostatic and van der Waal interactions. As shown in Table 8, the interaction of water with calcite is over three times stronger than that with silica. As the pore becomes smaller, the interactions become more attractive, which corroborates the reduction in CO_2 solubility.

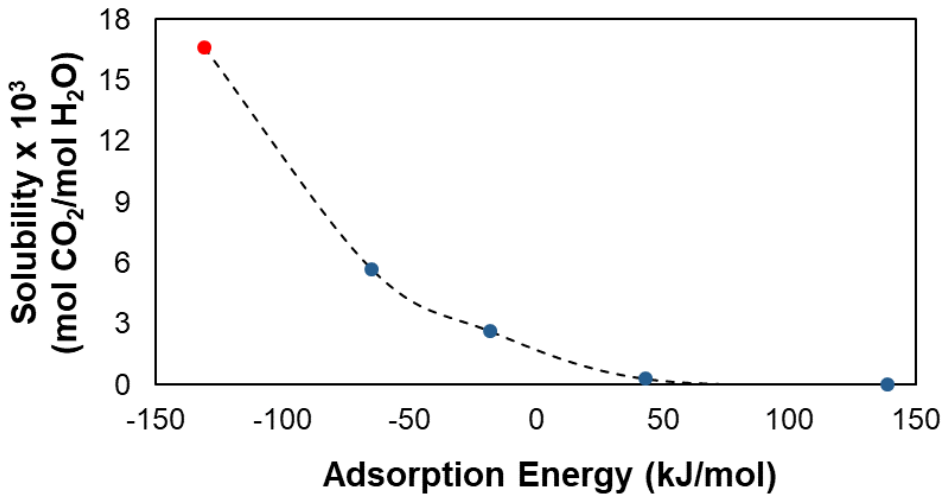

Figure 7. Relationship between CO_2 solubility (in bulk water (red) and water confined in calcite pores (blue)) and adsorption energy. The simulated temperature was 323 K. The line is a guide to the eye.

Table 8. Interaction energy between water and the simulated mineral surfaces at 323 K.

		Water-Surface E_{int} (kJ/mol)
Silica	3nm	-5.3
Calcite	3nm	-17.5
	2.8 nm	-18.4
	2.5 nm	-19.9
	2 nm	-25.2

We also calculated interaction energies (E_{int}) between CO_2 and water/ions in the various systems considered. We normalized the results to represent one CO_2 molecule interacting with 2000 water molecules. The results, presented in Table 9, show that confinement reduces the attraction between CO_2 and the aqueous solution by almost 50%, compared to the bulk. The ions lead to stronger attractions, but the effect is somewhat more pronounced in the bulk than in confinement. The slightly stronger attractions between CO_2 and the aqueous systems in confinement does not seem to explain the differences in solubility discussed above, which is probably due to the different distributions of the electrolytes within the pore. Ho and Ilgen[9] observed that the dominant contribution to the hydration of CO_2 is the formation of molecular cavities. Our density distribution results show that CO_2 in confined water accumulates in the center of the pore. Because cavities are less likely to form within dense hydration layers, our results seem consistent with the observations of Ho and Ilgen[9], although a detailed analysis of the mechanisms responsible for the energetics in our systems has not been carried out.

Table 9. Interaction energy between CO_2 and aqueous systems in bulk and in 3 nm pores at 323 K.

	Salinity	CO_2-Water/Ion E_{int} (kJ/mol)
Bulk	0	-23.7 ± 0.0
	1.5 M NaCl	-24.8 ± 0.2
	1.5 M $MgCl_2$	-25.5 ± 0.1
Confined	0	-13.1 ± 1.5
	1.5 M NaCl	-13.6 ± 1.5
	1.5 M $MgCl_2$	-13.9 ± 0.0

3.4. Transport Properties

To evaluate the transport properties of CO_2 in the hydrated pores and compare them to the corresponding bulk properties, we use the Einstein relation to compute the self- diffusion coefficients,[57,58] following the approaches implemented previously in the group.[17,56,59,60]

We calculated the overall diffusion coefficient (D_{XYZ}) for CO_2 in bulk and the 2-D diffusion coefficients for CO_2 in confined systems (D_{XY}). The results, presented in Tables 10 and 11, suggest that at 303 K, the diffusion of CO_2 in the 3 nm pore is about an order of magnitude slower than that in the bulk, and that the CO_2 diffusion coefficient reduces further as the pore becomes smaller. Compared to region 2 (first layer of CO_2, Figure 3), the diffusion in the middle of the pore (region 3) is faster, as expected because water molecules in the first and second hydration layer should be less mobile than those in the middle of the pore.[61] Both NaCl and $MgCl_2$ are found to reduce the self-diffusion coefficients of CO_2 in water, both in confined and bulk systems.

It is perhaps useful to compare the 2D diffusion coefficients estimated for CO_2 in confined water to those previously reported for CH_4 in confined water.[56] In both cases, the same force field was used to describe water-calcite interactions. The difference is that the study for CH_4 referred to a 1 nm – wide slit shaped pore at 300 K, while we are considering here pores of width larger than 2.5 nm at 303 K. It was found that the diffusion coefficient of methane in hydrated calcite is over three times slower than that in hydrated silica pores. While a direct comparison cannot be made due to the significant difference in the pore width, it is likely that comparatively strong calcite-water as opposed to silica-water interactions are responsible for both the delayed diffusion of CH_4 in hydrated pores.

Table 10. Two-dimensional diffusion coefficients of CO_2 in water confined in calcite pores at 303 K.

System	Confined D_{xy} /x10^9 m^2s^{-1}	Confined D_{xy} in region 2 /x10^9 m^2s^{-1}	Confined D_{xy} in region 3 /x10^9 m^2s^{-1}
Pure water (3 nm)	2.5 ± 0.3	1.1 ± 0.06	2.5 ± 0.2
Pure water (2.8 nm)	1.8 ± 0.2	0.9 ± 0.1	2.1 ± 0.06
Pure water (2.5 nm)	1.7 ± 0.1	0.8 ± 0.06	2.0 ± 0.05
1.5 M NaCl (3 nm)	1.4 ± 0.2	0.8 ± 0.04	1.8 ± 0.02
1.5 M $MgCl_2$ (3 nm)	1.3 ± 0.1	0.8 ± 0.06	1.4 ± 0.2

Table 11. Diffusion Coefficients of CO_2 in bulk water at 303 K.

System	Bulk D_{xyz} /x10^9 m^2s^{-1}
Pure water	22.0 ± 1.9
1.5 M NaCl	17.4 ± 3.1
1.5 M $MgCl_2$	16.5 ± 4.1

4. CONCLUSIONS

Equilibrium MD simulations probed the solubility of CO_2 in water and brine confined in calcite pores (2 – 3 nm) at 303 K and 323 K. At comparable salinities, the solubility is lower in the pores compared to that in the bulk. However, when confined in the calcite pores, the solubility of CO_2 is reduced by adding NaCl, but it is slightly increased by adding $MgCl_2$, which seems to correlate with the preferential distribution of the ions within the hydrated pores. In hydrated calcite pores narrower than 2.5 nm, there was no detectable adsorption of CO_2. Adsorption energy results indicate that narrower calcite pores are less attractive for the adsorption of CO_2. Although the structure of water assessed by atomic density profiles does not change qualitatively within the pores investigated, the attractive interactions between water and the pore surface become stronger in smaller pores. The dynamic properties, quantified by the self-diffusion coefficient of CO_2, showed that both confinement and presence of salt ions reduce the mobility of CO_2. Comparing our results to those present in the literature, it appears that the dissolution of CO_2 in confined water is strongly affected by solute/solvent-pore interactions. Different interaction strengths seem to account for disparities in the solubility of gases in fluids in sandstone, carbonate and clay reservoirs. Quantifying these effects is important for the optimisation of geological sequestration strategies, as they affect the storage capacity in a carbonate formation and the time required for injected CO_2 to transport through said formation.

ACKNOWLEDGEMENTS

The Authors acknowledge the financial support from the U.S. Department of Energy, Office of Basic Energy Sciences, under Contract No. DE-SC0006878 (Division of Chemical Sciences, Geosciences, and Biosciences), Geosciences Program. AA was supported by the UK EPSRC Centre for Doctoral Training in the Advanced Characterisation of Materials (Grant No.

EP/S023259/1). AS acknowledges financial support from the Science4CleanEnergy consortium (S4CE), which is supported by the Horizon2020 R&D programme of the European Commission, via grant No. 764810. We are also grateful to the University College London Research Computing Platforms Support (MYRAID, GRACE and KATHLEEN) for access to high-performance computing.

REFERENCES

1. Liu, Y.; Hou, M.; Yang, G.; Han, B. Solubility of CO2 in Aqueous Solutions of NaCl, KCl, CaCl2 and Their Mixed Salts at Different Temperatures and Pressures. *J Supercrit Fluids* **2011,** *56*, 125-129.
2. Emami-Meybodi, H.; Hassanzadeh, H.; Green, C. P.; Ennis-King, J. Convective Dissolution of CO2 in Saline Aquifers: Progress in Modeling and Experiments. *Int J Greenh Gas Control* **2015,** *40*, 238-266.
3. Gilbert, K.; Bennett, P. C.; Wolfe, W.; Zhang, T.; Romanak, K. D. CO2 Solubility in Aqueous Solutions ontaining Na+, Ca2+, Cl−, SO42− and HCO3-: The Effects of Electrostricted Water and Ion Hydration Thermodynamics. *Appl Geochemistry* **2016,** *67*, 59-67.
4. Yasunishi, A.; Yoshida, F. Solubility of carbon dioxide in aqueous electrolyte solutions. *J Chem Eng Data* **1979,** *24*, 11-14.
5. Pérez-Salado Kamps, Á.; Jödecke, M.; Xia, J.; Vogt, M.; Maurer, G. Influence of Salts on the Solubility of Carbon Dioxide in (Water + Methanol). Part 1: Sodium Chloride. *Ind Eng Chem Res* **2006,** *45*, 1505-1515.
6. Tong, D.; Trusler, J. P. M.; Vega-Maza, D. Solubility of CO2 in Aqueous Solutions of CaCl2 or MgCl2 and in a Synthetic Formation Brine at Temperatures up to 423 K and Pressures up to 40 MPa. *J Chem Eng Data* **2013,** *58*, 2116-2124.
7. Jacob, R.; Saylor, B. Z. CO2 Solubility in Multi-Component Brines Containing NaCl, KCl, CaCl2 and MgCl2 at 297K and 1–14MPa. *Chem Geol* **2016,** *424*, 86-95.
8. Yasunishi, A.; Yoshida, F. Solubility of Carbon Dioxide in Aqueous Eelectrolyte Solutions. *J Chem Eng Data* **1979,** *24*, 11-14.
9. Ho, T. A.; Ilgen, A. Density Fluctuation in Aqueous Solutions and Molecular Origin of Salting-Out Effect for CO2. *J Phys Chem B* **2017,** *121*, 11485-11491.
10. Phan, A.; Cole, D. R.; Striolo, A. Aqueous Methane in Slit-Shaped Silica Nanopores: High Solubility and Traces of Hydrates. *J Phys Chem C* **2014,** *118*, 4860-4868.
11. Phan, A.; Cole, D. R.; Striolo, A. Factors Governing the Behaviour of Aqueous Methane in Narrow Pores. *Phil Trans R Soc A* **2016,** *374*, 20150019.
12. Ho, L. N.; Schuurman, Y.; Farrusseng, D.; Coasne, B. Solubility of Gases in Water Confined in Nanoporous Materials: ZSM-5, MCM-41, and MIL-100. *J Phys Chem C* **2015,** *119*, 21547-21554.
13. Diaz Campos, M.; Akkutlu, I. Y.; Sigal, R. F. *A Molecular Dynamics Study on Natural Gas Solubility Enhancement in Water Confined to Small Pores*, SPE Annual Technical Conference and Exhibition, New Orleans, Louisiana,2009; Society of Petroleum Engineers, 2009.
14. Luzar, A.; Bratko, D. Gas Solubility in Hydrophobic Confinement. *J Phys Chem B* **2005,** *109*, 22545-22552.

15. Bratko, D.; Luzar, A. Attractive Surface Force in the Presence of Dissolved Gas: A Molecular Approach. *Langmuir* **2008,** *24*, 1247-1253.
16. Pera-Titus, M.; El-Chahal, R.; Rakotovao, V.; Daniel, C.; Miachon, S.; Dalmon, J.-A. Direct Volumetric Measurement of Gas Oversolubility in Nanoliquids: Beyond Henry's Law. *ChemPhysChem* **2009,** *10*, 2082-2089.
17. Badmos, S. B.; Striolo, A.; Cole, D. R. Aqueous Hydrogen Sulfide in Slit-Shaped Silica Nanopores: Confinement Effects on Solubility, Structural, and Dynamical Properties. *J Phys Chem C* **2018,** *122*, 14744-14755.
18. Liu, Y.; Panagiotopoulos, A. Z.; Debenedetti, P. G. Monte Carlo Simulations of High-Pressure Phase Equilibria of CO2–H2O Mixtures. *J Phys Chem B* **2011,** *115*, 6629-6635.
19. Mitchell, M. J.; Jensen, O. E.; Cliffe, K. A.; Maroto-Valer, M. M. A Model of Carbon Dioxide Dissolution and Mineral Carbonation Kinetics. *Proc Math Phys Eng Sci* **2010,** *466*, 1265-1290.
20. Aminov, D.; Pines, D.; Kiefer, P. M.; Daschakraborty, S.; Hynes, J. T.; Pines, E. Intact Carbonic Acid is a Viable Protonating Agent for Biological Bases. *Proc Natl Acad Sci USA* **2019,** *116*, 20837-20843.
21. Gadikota, G.; Dazas, B.; Rother, G.; Cheshire, M. C.; Bourg, I. C. Hydrophobic Solvation of Gases (CO2, CH4, H2, Noble Gases) in Clay Interlayer Nanopores. *J Phys Chem C* **2017,** *121*, 26539-26550.
22. Botan, A.; Rotenberg, B.; Marry, V.; Turq, P.; Noetinger, B. Carbon Dioxide in Montmorillonite Clay Hydrates: Thermodynamics, Structure, and Transport from Molecular Simulation. *J Phys Chem C* **2010,** *114*, 14962-14969.
23. Li, W.; Nan, Y.; Zhang, Z.; You, Q.; Jin, Z. Hydrophilicity/Hydrophobicity Driven CO2 Solubility in Kaolinite Nanopores in Relation to Carbon Sequestration. *Chem Eng J* **2020,** *398*, 125449.
24. Tenney, C. M.; Cygan, R. T. Molecular Simulation of Carbon Dioxide, Brine, and Clay Mineral Interactions and Determination of Contact Angles. *Environ Sci Technol* **2014,** *48*, 2035-2042.
25. Li, W.; Nan, Y.; You, Q.; Jin, Z. CO2 Solubility in Brine in Silica Nanopores in relation to Geological CO2 Sequestration in Tight formations: Effect of Salinity and pH. *Chem Eng J* **2020,** *411*, 127626.
26. Ikeda, T.; Boero, M.; Terakura, K. Hydration of Alkali Ions from First Principles Molecular Dynamics Revisited. *J Chem Phys* **2007,** *126*, 034501.
27. Helm, L.; Merbach, A. E. Water Exchange on Metal Ions: Experiments and Simulations. *Coord Chem Rev* **1999,** *187*, 151-181.
28. Parmar, A. S.; Muschol, M. Hydration and Hydrodynamic Interactions of Lysozyme: Effects of Chaotropic versus Kosmotropic Ions. *Biophys J* **2009,** *97*, 590-598.
29. Marcus, Y. Effect of Ions on the Structure of Water: Structure Making and Breaking. *Chem Rev* **2009,** *109*, 1346-1370.
30. Mancinelli, R.; Botti, A.; Bruni, F.; Ricci, M. A.; Soper, A. K. Hydration of Sodium, Potassium, and Chloride Ions in Solution and the Concept of Structure Maker/Breaker. *J Phys Chem B* **2007,** *111*, 13570-13577.
31. Kerisit, S.; Parker, S. C. Free Energy of Adsorption of Water and Metal Ions on the {10$\bar{1}$4} Calcite Surface. *J Am Chem Soc* **2004,** *126*, 10152-10161.
32. Michael, K.; Golab, A.; Shulakova, V.; Ennis-King, J.; Allinson, G.; Sharma, S.; Aiken, T. Geological Storage of CO2 in Saline Aquifers—A Review of the Experience from Existing Storage Operations. *Int J Greenh Gas Control* **2010,** *4*, 659-667.
33. Green, D. W.; Perry, R. H. *Perry's Chemical Engineers' Handbook;* McGraw-Hill Education: New York, 2008.

34. Zhu, A.; Zhang, X.; Liu, Q.; Zhang, Q. A Fully Flexible Potential Model for Carbon Dioxide. *Chin J Chem Eng* **2009,** *17*, 268-272.
35. Xiao, S.; Edwards, S. A.; Grater, F. A New Transferable Forcefield for Simulating the Mechanics of CaCO3 Crystals. *J Phys Chem C* **2011,** *115*, 20067-20075.
36. Ali, A.; Le, T. T. B.; Striolo, A.; Cole, D. R. Salt Effects on the Structure and Dynamics of Interfacial Water on Calcite Probed by Equilibrium Molecular Dynamics Simulations. *J Phys Chem C* **2020,** *124*, 24822-24836.
37. Berendsen, H. J. C.; Grigera, J. R.; Straatsma, T. P. The Missing Term in Effective Pair Potentials. *J Phys Chem* **1987,** *91*, 6269-6271.
38. Joung, I. S.; Cheatham, T. E. Determination of Alkali and Halide Monovalent Ion Parameters for Use in Explicitly Solvated Biomolecular Simulations. *J Phys Chem B* **2008,** *112*, 9020-9041.
39. Duboué-Dijon, E.; Mason, P. E.; Fischer, H. E.; Jungwirth, P. Hydration and Ion Pairing in Aqueous Mg2+ and Zn2+ Solutions: Force-Field Description Aided by Neutron Scattering Experiments and Ab Initio Molecular Dynamics Simulations. *J Phys Chem B* **2018,** *122*, 3296-3306.
40. Pluhařová, E.; Fischer, H. E.; Mason, P. E.; Jungwirth, P. Hydration of the Chloride Ion in Concentrated Aqueous Solutions using Neutron Scattering and Molecular Dynamics. *Mol Phys* **2014,** *112*, 1230-1240.
41. Pluhařová, E.; Mason, P. E.; Jungwirth, P. Ion Pairing in Aqueous Lithium Salt Solutions with Monovalent and Divalent Counter-Anions. *J Phys Chem A* **2013,** *117*, 11766-11773.
42. Cygan, R. T.; Romanov, V. N.; Myshakin, E. M. Molecular Simulation of Carbon Dioxide Capture by Montmorillonite Using an Accurate and Flexible Force Field. *J Phys Chem C* **2012,** *116*, 13079-13091.
43. Chen, C.; Zhang, N.; Li, W.; Song, Y. Hydrogen Bonds at Silica–CO2 Saturated Water Interface under Geologic Sequestration Conditions. *Mol Phys* **2016,** *114*, 2924-2935.
44. Zhao, L.; Lin, S.; Mendenhall, J. D.; Yuet, P. K.; Blankschtein, D. Molecular Dynamics Investigation of the Various Atomic Force Contributions to the Interfacial Tension at the Supercritical CO2–Water Interface. *J Phys Chem B* **2011,** *115*, 6076-6087.
45. Hamm, L. M.; Bourg, I. C.; Wallace, A. F.; Rotenberg, B. Molecular Simulation of CO2- and CO3-Brine-Mineral Systems. *Rev Mineral Geochem* **2013,** *77*, 189-228.
46. Allen, M. P.; Tildesley, D. J. *Computer Simulation of Liquids;* Oxford University Press: Oxford, UK, 2004.
47. Darden, T.; York, D. M.; Pedersen, L. G. Particle Mesh Ewald: An N·log(N) Method for Ewald Sums in Large Systems. *J Chem Phys* **1993,** *98*, 10089.
48. Benavides, A. L.; Aragones, J. L.; Vega, C. Consensus on the Solubility of NaCl in Water from Computer Simulations using the Chemical Potential Route *J Chem Phys* **2016,** *144*, 124504.
49. Hess, B.; Kutzner, C.; van der Spoel, D.; Lindahl, E. GROMACS 4: Algorithms for Highly Efficient, Load-Balanced, and Scalable Molecular Simulation. *J Chem Theory Comput* **2008,** *4*, 435–447.
50. Van Der Spoel, D.; Lindahl, E.; Hess, B.; Groenhof, G.; Mark, A. E.; Berendsen, H. J. C. GROMACS: Fast, Flexible, and Free. *J Comput Chem* **2005,** *26*, 1701-1718.
51. Hoover, W. G. Canonical Dynamics : Equilibrium Phase-Space Distributions. *Phys Rev A* **1985,** *31*, 1695-1697.
52. Nose, S. A Molecular-Dynamics Method for Simulations in the Canonical Ensemble *Mol Phys* **1984,** *52*, 255-268.
53. Miyamoto, S.; Kollman, P. A. Settle: An Analytical Version of the SHAKE and RATTLE Algorithm for Rigid Water Models *J Comput Chem* **1992,** *13*, 952–962.

54. Heinz, H. Computational Screening of Biomolecular Adsorption and Self-Assembly on Nanoscale Surfaces. *J Comput Chem* **2010,** *31*, 1564-1568.
55. Phan, A.; Striolo, A. Evidence of Facilitated Transport in Crowded Nanopores. *J Phys Chem Lett* **2020,** *11*, 1814-1821.
56. Bui, T.; Phan, A.; Cole, D. R.; Striolo, A. Transport Mechanism of Guest Methane in Water-Filled Nanopores. *J Phys Chem C* **2017,** *121*, 15675-15686.
57. Gubbins, K. E.; Liu, Y.-C.; Moore, J. D.; Palmer, J. C. The Role of Molecular Modeling in Confined systems: Impact and Prospects. *Phys Chem Chem Phys* **2011,** *13*, 58-85.
58. Kinaci, A.; Haskins, J. B.; Çağın, T. On Calculation of Thermal Conductivity from Einstein Relation in Equilibrium Molecular Dynamics. *J Chem Phys* **2012,** *137*, 014106.
59. Apostolopoulou, M.; Santos, M. S.; Hamza, M.; Bui, T.; Economou, I. G.; Stamatakis, M.; Striolo, A. Quantifying Pore Width Effects on Diffusivity via a Novel 3D Stochastic Approach with Input from Atomistic Molecular Dynamics Simulations. *J Chem Theory Comput* **2019,** *15*, 6907-6922.
60. Argyris, D.; Cole, D. R.; Striolo, A. Dynamic Behavior of Interfacial Water at the Silica Surface. *J Phys Chem C* **2009,** *113*, 19591-19600.
61. Ho, T. A.; Argyris, D.; Cole, D. R.; Striolo, A. Aqueous NaCl and CsCl Solutions Confined in Crystalline Slit-Shaped Silica Nanopores of Varying Degree of Protonation. *Langmuir* **2012,** *28*, 1256-1266.

TOC GRAPHIC